Human cerebellar sub-millimeter diffusion imaging reveals the motor and non-motor topography of the dentate nucleus

Christopher J. Steele[1],*, Alfred Anwander[1], Pierre-Louis Bazin[1], Robert Trampel[1], Andreas Schaefer[1], Robert Turner[1], Narender Ramnani[2], and Arno Villringer[1]

[1] Max Planck Institute for Human Cognitive and Brain Sciences, Leipzig, Germany.

[2] Royal Holloway University of London, Psychology

* Corresponding author:

Christopher Steele

Max Planck Institute for Human Cognitive and Brain Sciences

Department of Neurology

Stephanstr. 1a, 04103 Leipzig, Germany

Phone: +49 341 9940 2207

http://www.cbs.mpg.de/employees/steele

Abstract

The reciprocal cortico-cerebellar loops that underlie cerebellar contributions to motor and cognitive behaviour form one of the largest systems in the primate brain. Work with non-human primates has shown that the dentate nucleus, the major output nucleus of the cerebellum, contains topographically distinct connections to both motor and non-motor regions, yet there is no evidence for how the cerebellar cortex connects to the dentate nuclei in humans. Here we used in-vivo submillimeter diffusion imaging to characterise this fundamental component of the cortico-cerebellar loop, and identified a pattern of superior motor and infero-lateral non-motor connectivity strikingly similar to that proposed by animal work. Crucially, we also present first evidence that the dominance for motor connectivity observed in non-human primates may be significantly reduced in man – a finding that is in accordance with the proposed increase in cerebellar contributions to higher cognitive behaviour over the course of primate evolution.

Keywords

Introduction

Invasive tract-tracing in non-human primates has revealed a dense pattern of reciprocal connectivity between the cerebral cortex, cerebellar cortex, and cerebellar nuclei that defines cerebellar contributions to behaviour (Kelly and Strick 2003; Ramnani 2006). These cortico-cerebellar loops form one of the largest systems in the primate brain and, while traditionally thought of as influencing only motor function, we are now beginning to understand their contributions to higher cognitive function and emotion (Ramnani 2006; Schmahmann et al. 2009; Strick et al. 2009; Stoodley and Schmahmann 2010). Specifically, there is evidence from non-human primates that the dentate nucleus, the largest output nucleus of the cerebellum, exhibits a topographical organization of projections to motor and non-motor cortex: with rostro-dorsal regions projecting to motor cortex and ventro-lateral regions to prefrontal and parietal cortex (Middleton and Strick 2001; Dum and Strick 2003; Strick et al. 2009). A similar topographical organisation of dentate nuclear motor vs non-motor connectivity has also been shown in human functional imaging studies (Küper et al. 2011; Thürling et al. 2011; Bernard et al. 2014). Crucially, the projections from the dentate nucleus in humans are thought to differ from those of non-human primates in a manner consistent with the expanded role of the prefrontal cortex in human evolution (Ramnani et al. 2006), but how the white-matter of the cerebellar cortex projects to the dentate nucleus is entirely unknown. Thus, though the cerebellum has undergone important evolutionary change and serves as the "heart" of the brain – connecting to and supporting brain function primarily through the dentate nucleus – *"There is no evidence on the cortico-nuclear projection of the human cerebellar hemisphere"* (Voogd et al. 2013). Over the past fifteen years, many studies have provided evidence that the cerebellum is involved in both motor and non-motor behaviour (Ramnani 2006; Schmahmann et al. 2009; Stoodley and Schmahmann 2009, 2010; Marvel and Desmond 2010). The cerebellum is thought to support cognition through multi-synaptic reciprocal loops with motor and non-motor regions of the cerebrum – distinctions which have been used to differentiate between motor and non-motor regions of cerebellar cortex and nuclei in non-human primates (Middleton and Strick 2001; Dum et al. 2002; Dum and Strick 2003; Kelly and Strick 2003; Strick et al. 2009). These putative motor and non-motor cerebellar cortical regions largely follow anatomical boundaries of adjacent lobules (according to the lobular definitions of Larsell 1970), with lobules HIV, V, and VI exhibiting the greatest proportion of motor connectivity, and Crus I and II that of non-motor connectivity (Kelly and Strick 2003). Though lobules HVIIB and VIII have also been shown to connect to the motor cortex in non-human primates, their connectivity accounted for only ~20% of the total connections with the motor cortex (Kelly and Strick 2003). Numerous studies in cerebellar lesion patients (Schmahmann et al. 2009; Stoodley and Schmahmann 2010; Bodranghien et al. 2016), and in healthy subjects employing task-based functional magnetic resonance imaging (fMRI) (Stoodley and Schmahmann 2009; Stoodley et al. 2012), and resting state fMRI (O'Reilly et al. 2010; Buckner et al. 2011) indicate that there may be a similar motor and non-motor distinction in the human cerebellum, though its exact nature is still debated (Glickstein and Doron 2008). Regardless of the potential functional implications of cerebellar connectivity, the present study utilises the

anatomical motor and non-motor distinctions between cerebellar cortical regions as defined by the anatomical connectivity work of Strick and colleagues (Kelly and Strick 2003).

Recent work has begun to characterise the global organisation of cerebellar fibres through dissection (Perrini et al. 2012; Akakin et al. 2014) and diffusion magnetic resonance imaging (dMRI) (Dell'Acqua et al. 2013; Takahashi et al. 2013) in ex-vivo samples, but has not addressed the connectivity between the cortex and nuclei. dMRI is a promising way to gain insight into white-matter structural connectivity in-vivo, providing a detailed mapping of tract trajectories and connectivity in the living human brain (Van Essen 2013). However, while non-invasive and relatively easy to perform, dMRI suffers from partial volume effects that make investigation of the cerebellum problematic. To reduce these limitations, we acquired the first sub-millimeter in-vivo diffusion images of the human cerebellum with a zoomed and parallel image acquisition using an ultra-high field at 7 Tesla MRI scanner (Heidemann et al. 2012). We used constrained spherical deconvolution to derive fibre orientation, a method known to be better at resolving crossing fibres (Tournier et al. 2007). We then performed targeted tractography between the cerebellar lobules and dentate nucleus, followed by tract-based surface classification. Seed masks were restricted to the cortical regions of each lobule to exclude the major white-matter bundles, and resulted in a probabilistic tractography path from individual cortical lobules to the dentate nucleus. We utilized these techniques to accurately capture the fine details of white-matter connectivity within a very small region of the brain – a feat that is not possible at lower field strengths (3T) or conventional diffusion imaging resolutions (1.7-3.0 mm isotropic).

In this study, we combined sub-millimeter dMRI with probabilistic tractography to determine the topographical organisation of cerebellar cortico-nuclear connectivity and to characterise the relative dominance of motor versus non-motor cortico-cerebellar loops in the living human brain.

Methods

Image acquisition

We conducted sub-millimeter isotropic diffusion-weighted magnetic resonance imaging (dMRI) of the cerebellum of 6 healthy young volunteers (4 females). All participants provided written informed consent in accordance with the research ethics board at the University of Leipzig. Imaging was performed on a 7T Siemens scanner equipped with a 24-channel head coil (MAGNETOM 7T, Siemens Healthineers, Magnetic Resonance, Erlangen, Germany). We used ZOOmed Partially Parallel Acquisition (ZOOPPA) to acquire dMRI data at 0.8 mm isotropic resolution of the cerebellum (Heidemann et al. 2012) (60 directions, 7 interspersed non diffusion-weighted b0 images, TR=13700ms , TE=68ms, b=1000 mm/s^2, GRAPPA=2, ZOOM=2.7, bandwidth=1034, 186x120 matrix, 78 slices centered on the cerebellum, four repetitions). Slice coverage is depicted in Figure

1 (left). Total acquisition time was approximately one hour. Individual T1-maps with 0.7 mm isotropic resolution were also acquired during a separate session for registration and segmentation of the cerebellar lobules (MP2RAGE: TI1/TI2 = 900/2750ms, TR = 5s, TE = 2.45ms, α1/α2 = 5°/3°, GRAPPA = 2) (Marques et al. 2010). Two overlapping 5mm thick high permittivity dielectric pads (Teeuwisse et al. 2012) were placed between the back of the head and the coil to further enhance signal quality on all scans. A graphical overview of the acquisition and processing methods is provided in Figure 1 (right).
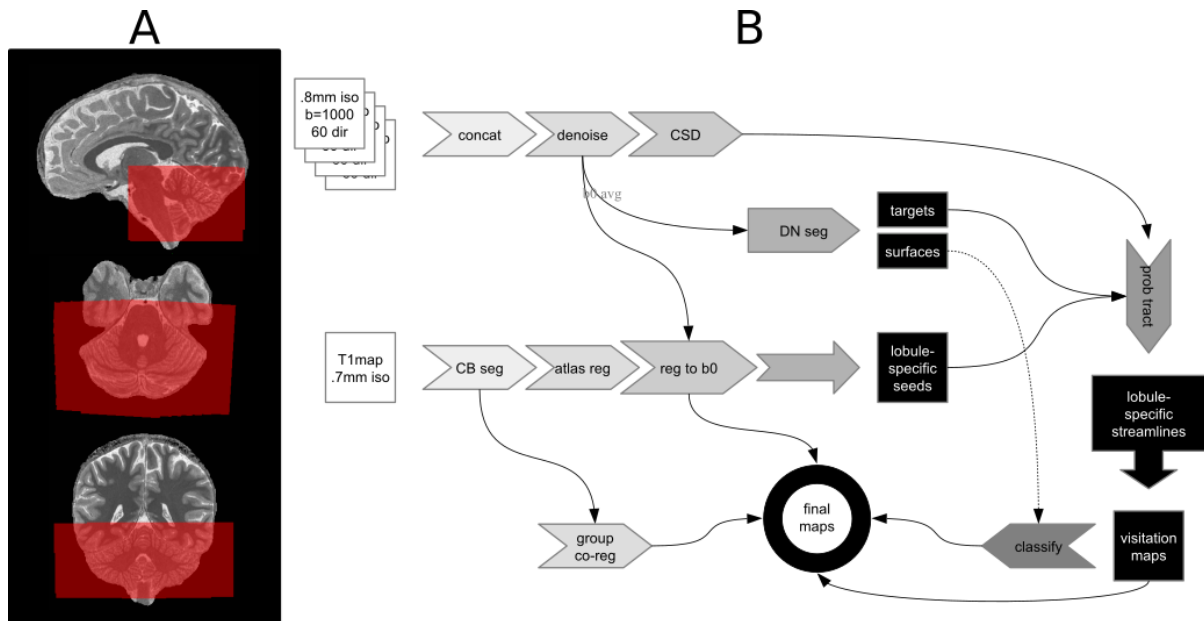
Figure 1. Overview of acquisition, data processing steps, and outputs.
Left panel: Slice coverage area of the dMRI sequence (white) overlaid on a whole-brain quantitative T1 map of a representative individual.
Right panel: Image processing and analysis pipeline. Raw data is depicted in white, processing steps in grey, intermediate outputs in black. The final maps represent the co-registered visitation maps and classified dentate nucleus surfaces.

dMRI preprocessing

Each participant's four separate diffusion acquisitions were concatenated and denoised with a four-dimensional local principal components filter (Manjón et al. 2013). MRtrix (http://www.nitrc.org/projects/mrtrix, version 0.2.11) was used to derive the fibre orientation density function (fODF (Tournier et al. 2007)) with constrained spherical deconvolution (CSD, spherical harmonics order of 8), generate fractional anisotropy (FA) images, perform probabilistic tractography, and compute tract-density images (Calamante et al. 2011). The single fibre response function necessary for CSD deconvolution was computed for each participant from voxels with FA > 0.7 in the anterior portion of the left middle cerebellar peduncle (MCP).

Dentate nucleus target masks

The dentate nuclei (DN) were manually segmented using the average b0 anatomical images with the levelset based VOI tool implemented in the MIPAV software package (http://mipav.cit.nih.gov (McAuliffe et al. 2001)). Segmented DN masks were then topologically corrected and refined based on b0 image intensities and curvature constraints in a custom pipeline with the CBS Tools in MIPAV-JIST (http://www.cbs.mpg.de/institute/software/cbs-tools) (Lucas et al. 2012; Bazin et al. 2014). The corrected masks were inspected and corrected for any edge bleeding. The final mask was upsampled to 0.4 mm isotropic resolution and eroded by a single voxel to create the outer and inner DN masks, respectively. The outer masks were used to derive the DN average template (described below) and the inner masks were used as targets for probabilistic tractography.

To allow overlays and comparison of results in a common space, we created a study-specific group template made up of co-registered cerebellum (CB) FA maps using the Advanced Normalization Tools (ANTs, single linear [12 dof] and eight nonlinear steps with the group template tool) (Avants et al. 2008). Native space outer DN segmentations were then warped into common space to create the average DN (1 mm smoothing, iso-value = 0.2). Native space voxel-wise tractography results were also warped into the common space for display and further analyses.

T1-map preprocessing and cerebellar atlas registration

T1-maps were first skull stripped, segmented, and the cerebellum and brainstem were extracted using the CBS Tools in MIPAV-JIST. The cerebellum and brainstem were registered to the b0 average image using an initial rigid (6 dof) then nonlinear registration using ANTs. Next, a separately created segmented cerebellar atlas (Larsell's parcellation of a twelve subject 0.5 mm average cerebellum) (Larsell 1970; Bazin et al. 2014) was linearly (12 dof) and nonlinearly registered to the native space T1-maps. The registrations were then combined and the atlas was warped into each subjects' native diffusion space. In each participant the cerebellar grey-matter (GM) was segmented using the CBS Tools, and the individual masks were warped into native diffusion space and masked with the cerebellar atlas to produce the final individual GM cerebellar atlases. This resulted in masks for lobules HIV, V, VI, and Crus I, Crus II (Figure 2). Lobules HVIIB and VIII were excluded due to signal dropout in this area (Figure S1).
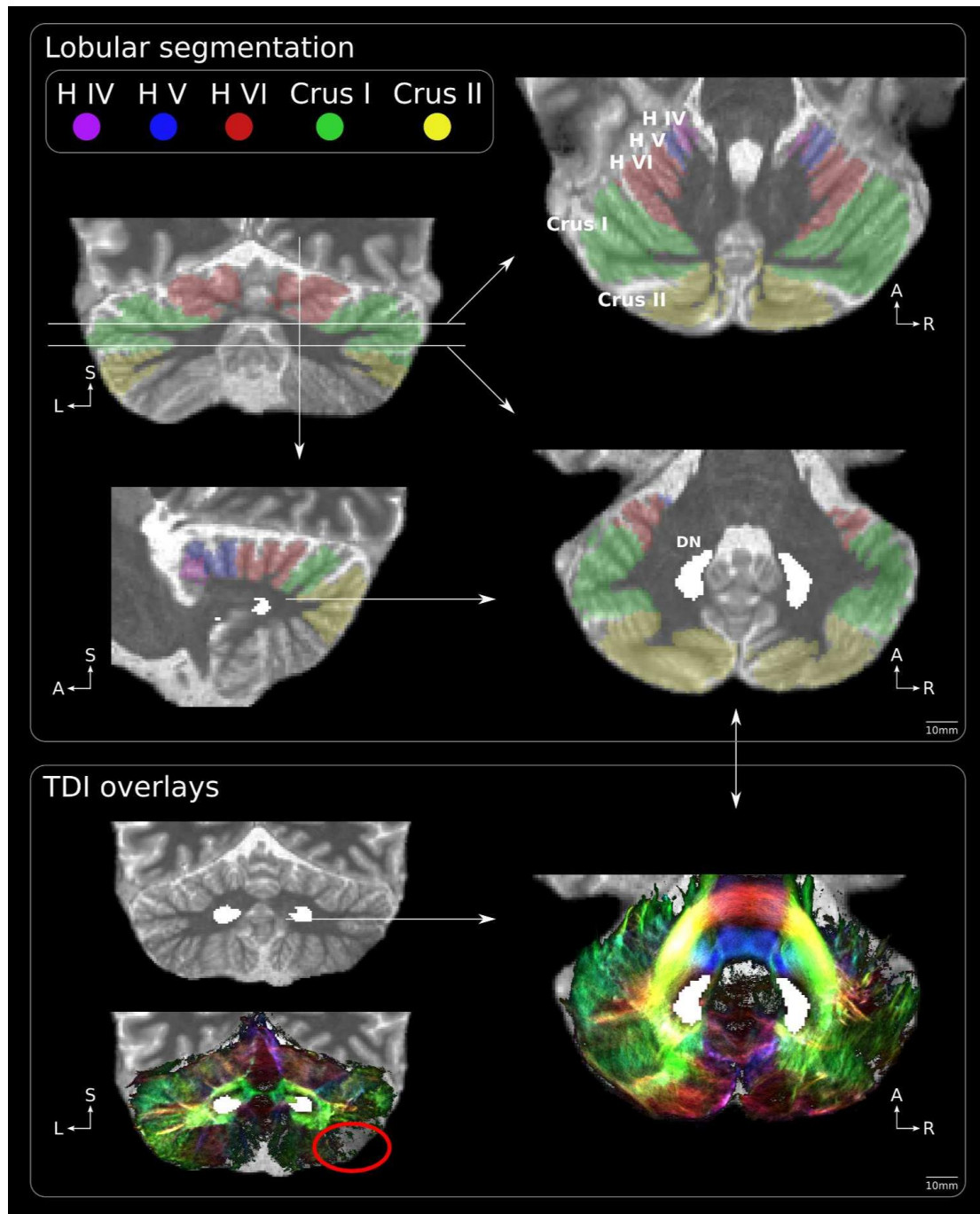
Figure 2. Seed masks and tract-density images (TDI). Lobular segmentation (top): Views of the lobular and dentate nucleus masks are presented as overlays on an individual's T1 map. The lobular colour code is the same for all images and slice markings (H IV – purple; H V – blue; H VI – red; Crus I – green; Crus II – yellow; dentate nucleus (DN) – white), and arrows indicate the position of slices. TDI overlays (bottom): Tract-density image overlayed on individual's T1 map. The red oval indicates a region of the postero-lateral cerebellum (lobule H VIII) where our acquisition had steep signal drop-off, resulting in a relative decrease in streamlines. TDI images follow standard orientation colour-coding (red: medial-lateral; blue: superior-inferior; green: anterior-posterior). Orientation legend: A – anterior; S – superior; L – left; R – right.

Cerebellar orientation and anatomical organisation

In the current paper, the anatomical terms used to refer cerebellar cortical regions follow Larsell's parcellation (Larsell 1970). In keeping with the literature on human brain organisation, we provide anatomical localisation with reference to the conventional anterior-posterior, superior-inferior, and medial-lateral axes when describing the results of the current study and other studies involving human subjects. The presentation and discussion of studies involving non-human animals follows the terminology for that literature: rostral-caudal, dorsal-ventral, and medial-lateral axes. The orientation of the human dentate nucleus presented in the current manuscript corresponds to that of non-human primates following the description of Dum and Strick (2003): anterior-posterior ~=rostral-caudal, superior-inferior ~= dorsal-ventral, medial-lateral ~= medial-lateral.

To create an overview for navigation and anatomical identification, tract-density images (TDI) of the cerebellum were created. Here, we seeded a total of five million probabilistic streamlines in all voxels with FA > 0.4 and FOD max > 0.1 (computed using CSD) and then supersampled the streamlines into colour-coded density images (0.2 mm isotropic voxels). We also performed a set of targeted tractography analyses to complement this analysis and confirm the relative arrangement of the cerebellar peduncles within the cerebellum. Here we set seed points in the superior, inferior, and middle cerebellar peduncles (SCP, ICP, MCP) (Figure 4). We performed probabilistic CSD tractography using 10,000 streamlines from each seed region, with a DN target mask (SCP), and target masks for the entire cerebellar cortex (ICP, MCP). These analyses were performed to provide the overall picture of the main fibre trajectories within the cerebellum, along with the more specific trajectories of the cerebellar peduncles, to enable comparison with previous tractography work in the human cerebellum (Granziera et al. 2009; van Baarsen et al. 2016). The following lobulespecific analysis was designed to identify the pattern of cortico-nuclear connectivity of the human cerebellum.

Lobule-specific probabilistic tractography to the dentate nucleus

To test whether the human cerebellum shows a topographically consistent pattern of cortico-nuclear connectivity that is similar to that found in nonhuman primates, we performed individual lobulespecific cortico-nuclear tractography between lobules HIV, V, VI, and Crus I and II and the dentate nucleus in both hemispheres. Lobule masks were set as the seed masks and the inner DN mask as the target, with individual-specific coronal exclusion masks in the cerebellar peduncles and axially in the brainstem above the SCP and below the ICP. This arrangement of masks ensured that only those streamlines directly connecting the lobules and dentate nuclei would be preserved. The total number of streamlines connecting each lobule to the DN was normalised according to the volume of the largest lobule in each individual. This normalisation step is akin to correcting for total brain volume in a voxel-based morphometry analysis – it prevents individuals with overly large or small brains from biasing the results and allows the data

to directly combined or compared. Tractography from the largest lobule was set at 50,000 successfully completed streamlines and, for example, a lobule that was half as large would be set at 25,000. We also set an initial FOD seeding threshold of 0.1 and a termination threshold of 0.1, terminated tractography upon entry of the target mask, and generated streamlines randomly throughout the seed volume. These parameters were chosen to seed from the GM of individual lobules with proper termination within the DN, and to ensure that a streamline entering one region of the DN did not continue through to another region. We adjusted the number of streamlines connecting each lobule to the DN by lobular volume to ensure that the representation of the connectivity of the DN was as unbiased as possible. With this method each lobule projects a different number of computed streamlines to the DN, but projects the same number of streamlines per voxel as every other lobule. Thus, ten streamlines from lobule HIV terminating in the DN are equivalent and comparable to ten streamlines from Crus II. The resulting lobulespecific streamlines were counted and resampled to create 0.2 mm isotropic voxel-wise visitation maps, which were used for individual classification or warped to the FA template space for group classification.

Lobule-specific classification of the dentate nucleus

Cerebellar cortico-nuclear connectivity was mapped with a two-pronged approach to assess both individual and grouped data. First, we submitted the individual native space lobule-specific visitation maps to a winner-takes-all voxel classification algorithm (Behrens et al. 2003) implemented in Python. The resulting maps were thresholded to include only those voxels containing a total of ten or more streamlines (at 0.2mm isotropic resolution). The proportion of motor (lobules HIV, V, VI) and non-motor (Crus I, II) territories on the surface of the DN was then calculated based on the projection of each classification onto the surface of individual DN (CBS Tools). In a second approach, the lobule-specific visitation maps were normalised to the template, thresholded to remove voxels with fewer than five streamlines, binarised, and summed across participants to create the population visitation maps. These maps were projected onto the group mean DN for display. The individual normalised lobule-specific visitation maps were also averaged across participants and submitted to the same classification approach described above to create the group average DN classification.

Confirmatory analyses

The potential effects of subject motion on our results were tested by replacing the 4d LPCA denoising step with a standard diffusion correction pipeline (Smith et al. 2004) and two-dimensional image noise reduction (Lohmann et al. 2010) and repeating the analyses.

Results

dMRI coverage extended from below the inferior olives to 10-20 mm within the occipital cortex, included the entire cerebellum, and extended anteriorly to include the brainstem. In one participant, the anterior portion of the brainstem was cut-off and only three quarters of the pons was within the field of view. The mean of the denoised b0 images for each subject are presented in Figure S1 of the supplementary materials, along with the derived motion correction parameters (Tables S1 and S2). Only three of the four dMRI acquisitions could be completed with two participants due to time limitations.

The segmented DN volumes were virtually identical to recently reported values. The mean volumes (± standard deviation) of the DN identified in this study were 385.0 ± 77.4 mm^3 for the left DN and 352.1 ± 72.2 mm^3 for the right, with an overall mean of 368.6 ± 73.4 mm^3. This fits well with the 362.8 ± 89.2 mm^3 and 366.1 ± 85.2 mm^3 identified by Diedrichsen and colleagues (2011) in susceptibility weighted images with 0.5 mm isotropic resolution and the 358 mm^3 found with reconstruction from 0.06 mm resolution post-mortem slices (Sultan et al. 2010). Previous MRIbased quantifications at lower resolutions have reported significantly larger volumes, though these are likely overestimations due to partial volume effects (Dimitrova et al. 2002; Deoni and Catani 2007).

Cerebellar orientation and anatomical organisation

Tract-density images were created for each participant to provide high-resolution images of the fibre tracts in the cerebellum. The course of the cerebellar peduncles and their relationship to the dentate nuclei is apparent in these images, as shown in Figure 3. The dentate nuclei appear as hypo-intense kidney-shaped structures in the axial plane. Their centres are approximately 13 mm lateral to the midline and mid-way along the anterior-posterior and inferior-superior axes of the cerebellum. The superior cerebellar peduncles connect along the medial surface of the DN and course antero-superiorly to exit the cerebellum and continue up the brainstem. The middle cerebellar peduncles connect in the pons and travel posteriorly into the cerebellum – making up the bulk of the white-matter in this region. Once inside the cerebellum, the MCP fans out to connect to lobular cortex, with a significant proportion of the fibres continuing laterally to the DN and connecting to Crus I & II. The inferior cerebellar peduncles connect in the brainstem and enter the cerebellum lateral to the SCP and medial to the MCP. The fibres travel superiorly, adjacent to the anterior pole of the DN, prior to fanning out and terminating in the cortex. The slices in the middle row of Figure 3 show that the posterior region of the cerebellar cortex, approximately equivalent to Crus I and II, is predominantly comprised of fibres running laterally across the cortex (shown in red). This pattern likely represents the parallel fibres of the cerebellar cortex (Dell'Acqua et al. 2013; Takahashi et al. 2013), and is not as pronounced in the more anterior lobules due to the more anterior-posterior orientation of these lobules relative to the sagittal plane. Navigable tract-density images for all participants in this study can be found at http://openscience.cbs.mpg.de/cerebellum. We also seeded in regions of the SCP, ICP

and MCP to confirm the relative arrangement of the cerebellar peduncles within the cerebellum (Figure 4). These results confirmed the pattern of connectivity described above, and is in agreement with the anatomical connectivity of the human cerebellum described by others with in-vivo dMRI (Granziera et al. 2009; van Baarsen et al. 2016), ex-vivo dMRI and histology (Dell'Acqua et al. 2013; Takahashi et al. 2013; Mollink et al. 2015), and recent dissection studies (Perrini et al. 2012; Akakin et al. 2014).
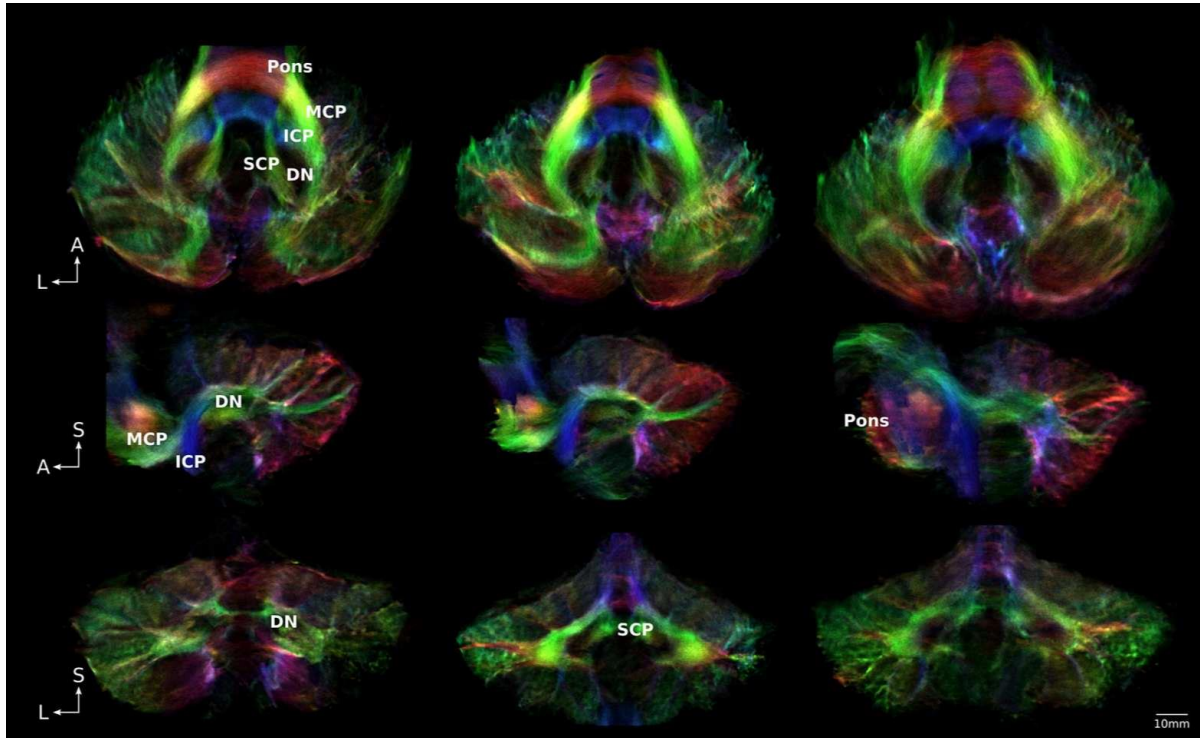
Figure 3. Tract-density images (TDI) of the human cerebellum at 0.2 mm (isotropic) in three participants. The major tracts, sub-cortical structures, and fine details of tract trajectories can be easily identified. A large amount of structure is visible in the sagittal slice through the pons (middle-right). The pronounced red colouration in the posterior regions of the cerebellar cortex is likely due to the medio-lateral alignment of parallel structures in the cerebellar cortex. All TDI images follow standard orientation colour-coding (red: medial-lateral; blue: superior-inferior; green: anterior-posterior). DN: dentate nucleus; SCP, MCP, ICP: superior, middle, inferior cerebellar peduncles. Orientation legend: A – anterior; S – superior; L – left.

### *Lobule-specific classification of the dentate nucleus*

Lobule-specific tractography to the dentate nucleus was successfully performed in all individuals. Streamlines exhibited a marked preference for connectivity that was topographically-consistent with the arrangement of the cerebellar cortex – such that the more superior lobules HIV, V, and VI connect to the superior surface of the dentate nucleus while the more postero-laterally oriented Crus I and II primarily connect to the posterior and lateral surfaces.
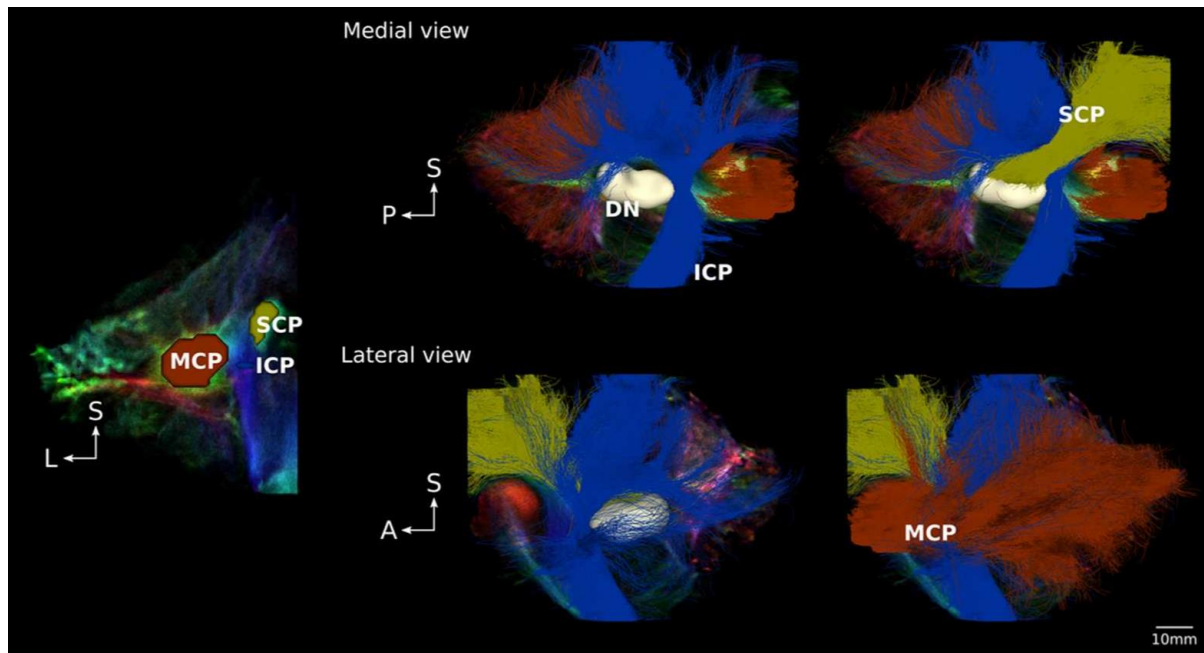
Figure 4. Delineation of the pathways of the cerebellar peduncles. Left: colour-coded seeds in the middle, superior, and inferior cerebellar peduncles (MCP=orange, SCP=gold, ICP=blue) are shown for a single subject. The four tractography images show Top: medial view of the ICP and MCP around the dentate nucleus with and without the SCP; Bottom: Lateral view with and without the MCP. Orientation legend: A – anterior; P – posterior; S – superior; L – left.

Individual classifications

The dentate nuclear surface area connected with each lobule across individuals and hemispheres was (mean ± standard deviation): HIV – 2.65 ± 1.52%, V – 4.82 ± 1.82%, VI – 12.85 ± 3.26%, Crus I – 17.65 ± 4.14%, Crus II – 16.51 ± 5.27%. Crucially, we found that a significantly greater area of the dentate nucleus was connected with the non-motor lobules of the cerebellar cortex (two-tailed paired t-test, $p < 0.001$, $t = 13.28$, df = 11; mean motor – 20.32 ± 3.66%; non-motor – 34.16 ± 4.89%. Since we projected from approximately 60% of the cerebellar volume in each individual, we expected that approximately 60% of dentate nuclear area would be classified. Our findings were as predicted, with 54.48 ± 5.76% of the area classified and 45.52 ± 5.76% unclassified. In addition, though the antero-superior region of the dentate nucleus that faces the medial axis where the SCP emerges was correctly left unlabelled in our analysis, it did contribute to our total surface calculation. We estimate that the SCP accounts for between 10 and 15% of what was identified as the total surface of the dentate nucleus. Assuming that the SCP accounts for a conservative 10% of total area, we infer that ~23% of the surface of the dentate nucleus was primarily connected with lobules HIV, V, and VI (motor), ~38% by Crus I and II (non-motor), and ~39% was not projected to by any of our seed regions – resulting in a non-motor:motor dominance ratio of 1.68 for the labelled regions.
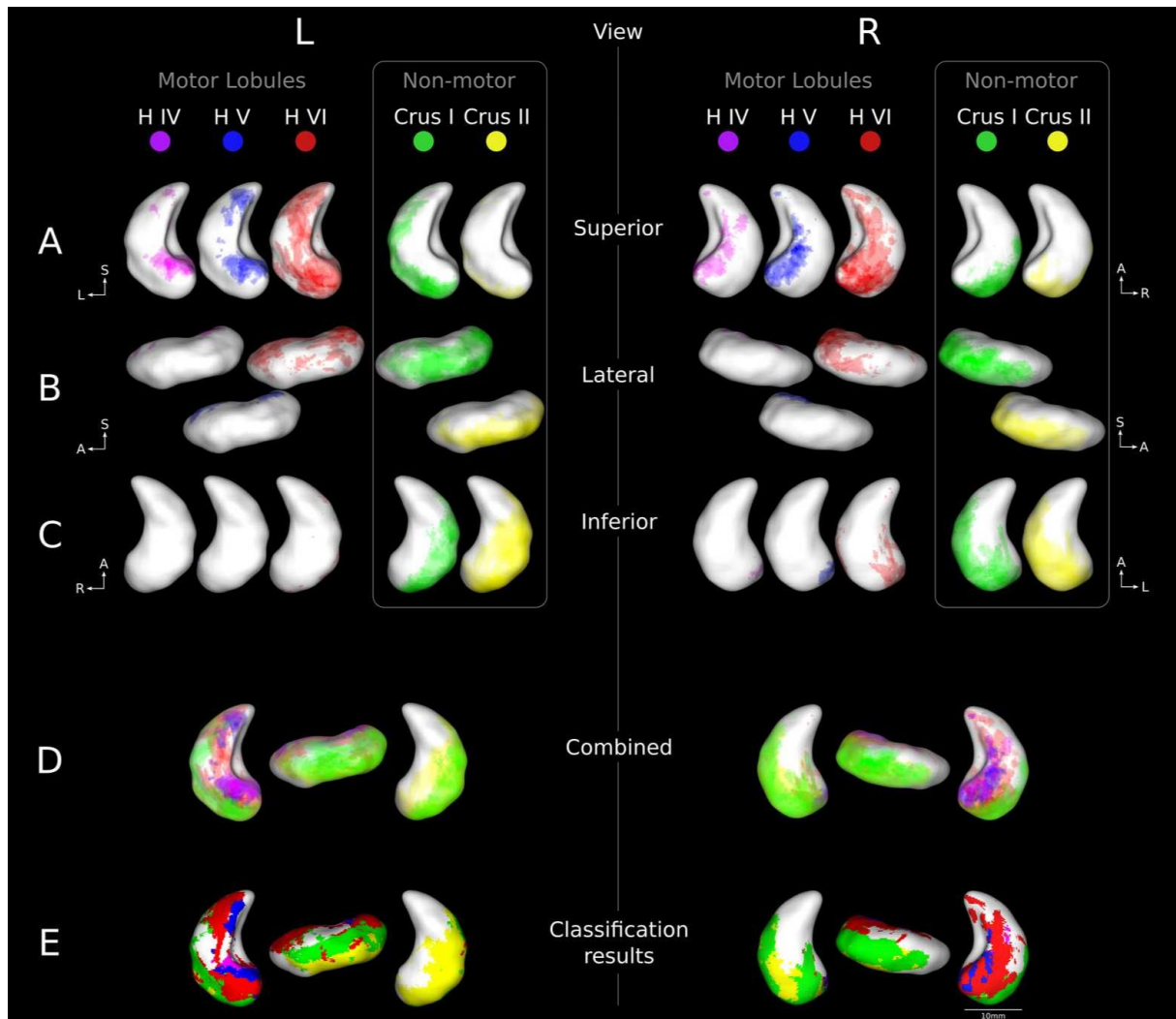
Figure 5. Group dentate nucleus visitation maps for the left (L) and right (R) hemispheres for the motor (HIV, V, VI) and non-motor (Crus I, II) lobules. Rows A-C: colour-coded visitation maps projected onto the mean dentate nucleus surface. Each lobule projection was thresholded to show connections consistent in two or more subjects. Superior, lateral, and inferior views of the dentate nucleus are shown separately for each lobule. The distinction between superior motor and infero-lateral non-motor is apparent. Row D: Overlay of group visitation maps showing the motor vs non-motor distinction. Row E: Dentate nuclear classification based on the group mean lobular connections. Both hemispheres show similar patterns of connectivity, with over 50% of the classified area primarily connected with non-motor lobules. The superior to infero-lateral distinction can also be seen clearly in this group classification map. Orientation legend: A – anterior; S – superior; L – left; R – right.
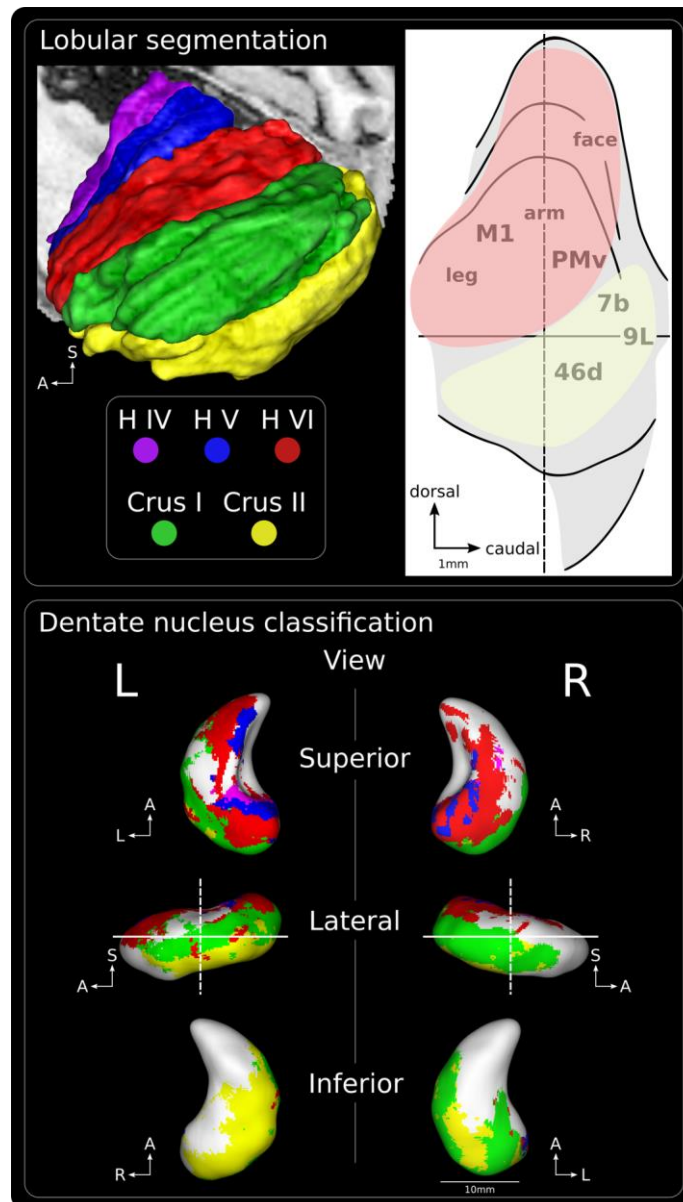
Figure 6. Relative dominance of non-motor connectivity (Crus I, II) in the human dentate nucleus. Top-left: Colour-coded cortical lobular segmentation. Bottom: classified images of the dentate nucleus of the left (L) and right (R) hemispheres. Dividing lines correspond to the surface separation along the superiorinferior(solid) and anterior-posterior dimensions (dotted), as in the image on the right. Our results show that the motor (HIV, V, VI) and non-motor (Crus I, II) territories of the human dentate nucleus occupy 20.3% and 34.2% of the total surface respectively. Top-right: unfolded map of the projections of the dentate nucleus in non-human primates, adapted from Dum and Strick (2003). The horizontal solid line in the middle of the image represents the lateral surface, which extends upwards (dorsally) or downwards (ventrally) along the dentate nucleus before curving medially towards the SCP. Red depicts the approximate rostro-dorsal motor and green the ventro-lateral zones of the dentate

nucleus (Strick et al., 2009). Orientation legend: A – anterior; S – superior; L – left; R – right.

Group visitation maps

We created a group visitation map of each lobule to depict the commonalities of the topographical relationship across subjects (Figure 5). Consistent with the streamline orientation present in the individual tractography maps, the group maps revealed that the superior surface was dominated by connections with the motor lobules HIV, V, and VI while the posterior and lateral surface was dominated by connections with the non-motor lobules Crus I and II. The inferior surface was also primarily connected to the non-motor lobules, albeit to a lesser extent. Interestingly, there was much more overlap present within the classifications (motor and non-motor) than between classifications – providing initial evidence that these connections are largely segregated.

Group classification map

In a final step, we created a group classification map by classifying the average of the co-registered individual visitation maps for each hemisphere. As with the findings from the group visitation maps, this analysis found that the superior surface of the dentate nucleus was dominated by connections with the motor lobules while the posterior and lateral surfaces were dominated by connections with the non-motor lobules (Figure 6). While strikingly similar to findings in nonhuman primates, which has established putative motor and non-motor territories (Strick et al. 2009), our work also shows that over 50% of the classified surface of the dentate nucleus is primarily connected with non-motor cerebellar cortical regions.

Confirmatory analyses

We found that replacing denoising with motion correction in our pipeline produced results that were virtually identical to those presented above. Figure S2 of the supplementary materials presents a summary of the visitation and classification results for direct comparison with Figure 5.

Discussion

We have used in-vivo sub-millimetre diffusion imaging to present the first structural evidence that the human dentate nucleus contains a superior motor and infero-lateral non-motor topographical connectivity similar to that proposed by animal work. Our findings are in good agreement with recent human functional imaging studies and support the idea of largely segregated cortico-cerebellar loops. In addition, we present first evidence that connections with non-motor cerebellar cortex are the dominant input to the human dentate nucleus. We found that cerebellar cortical non-motor connections took up ~1.68 times the classified surface area of motor connections – a finding that is in good agreement with the hypothesis of an expanded role of the cerebellum in supporting higher cognitive behaviour over the course of primate evolution.

Our findings present the first in-vivo structural evidence that the human dentate nucleus exhibits a connectivity topography that is similar to that of non-human animals. Previous research in animals suggests that the cortico-nuclear projections of the cerebellum follow a regular pattern of connectivity. In the first detailed study of cortico-nuclear connectivity, Clarke and Horsley (1905) found that cerebellar cortical ablation in cats led to selective degradation in the ipsilateral cerebellar nucleus closest to the lesion. This seminal work suggested that the cerebellum follows a general wiring principle where the dominant projections exist between adjacent cortical and nuclear regions. Using a similar approach, Jansen and Brodal (1940) comprehensively evaluated cortico-nuclear connectivity to create a set of degeneration maps of projections to the nuclei – providing the first evidence that there is a topographical map in the deep cerebellar nuclei that reflects the arrangement of the cerebellar cortex (also see Chan-Palay 1977). More recently, an elegant set of experiments performed by Strick and colleagues used invasive tractography to comprehensively map multiple motor and non-motor cortico-cerebellar loops in non-human primates (Middleton and Strick 2001; Dum and Strick 2003). Based upon this work, Strick and colleagues proposed that the dentate nucleus contains a predominantly rostro-dorsal motor and ventro-lateral non-motor pattern of reciprocal structural connectivity (Strick et al. 2009). Our results complement and extend this work by providing the first evidence for a similar topographical distribution of white-matter connectivity in humans.

In parallel, a large body of work in humans by Schmahmann and colleagues (Schmahmann et al. 2009; Stoodley and Schmahmann 2009, 2010; Stoodley et al. 2012), as well as others (O'Reilly et al. 2010; Buckner et al. 2011; Küper et al. 2011; Thürling et al. 2011; Adamaszek et al. 2014; Bernard et al. 2014), has provided converging evidence that different lobules of the cerebellar cortex are preferentially involved in motor and non-motor tasks. The few studies that have mapped functional activity in the dentate nucleus provide evidence for a predominantly antero-superior motor and postero-inferior non-motor division in humans (Küper et al. 2011; Thürling et al. 2011; Bernard et al. 2014). Küper and colleagues mapped motor (finger tapping) and cognitive (working memory and a visuospatial tasks) performance to antero-superior and posterior dentate nucleus, respectively (2011). Thürling and colleagues found that

motor speech activated the antero-superior region while verb generation was localised to the postero-inferior region of the dentate nucleus (2011). In a more data-driven manner, Bernard and colleagues recently compared the functional connectivity of seeds in superior and inferior dentate nucleus during rest (2014). Seeding in the superior dentate nucleus recruited predominantly anterior cerebellum (lobules I-IV, V, and VI, with activity extending into Crus I) while the inferior dentate recruited primarily posterior cerebellum (primarily Crus II) (Bernard et al. 2014). The authors identified two distinct motor and cognitive networks in the cerebellum and cerebral cortex that are consistent with those identified by Dum and Strick (Dum and Strick 2003) and are in excellent agreement with the cortico-nuclear connectivity that we have identified here.

Our findings provide further confirmation of the general superior vs inferior motor vs non-motor pattern of connectivity described in functional and patient work, confirms that the anterior and posterior cerebellum is predominately connected to the superior and inferior dentate nucleus respectively, and provides the first detailed assessment of white-matter cortico-nuclear connectivity in the human cerebellum. Our findings provide a description of the white-matter anatomical arrangement that may be useful for planning cerebellar surgery (Rhoton 2000), enhancing the interpretation of functional activity/connectivity in the cerebellum and dentate nucleus (O'Reilly et al. 2010; Buckner et al. 2011; Buckner 2013; Bernard et al. 2014), and could be used during interventional studies to help guide optimal electrode placement during non-invasive brain stimulation (Grimaldi et al. 2014; Sehm et al. 2014).

We found evidence for a pronounced distinction in motor vs non-motor white-matter connectivity in the human dentate nucleus. As previously discussed, this finding agrees with the structural anatomical findings from invasive tract tracing in non-human primates. However, there are important differences that provide additional evidence for the increased role of the human cerebellum in functions outside of the motor domain. In non-human primates, it has been estimated that 50-60% of the dentate nucleus is connected to motor-related regions (Dum and Strick 2003). In other words, non-human primates are estimated to have cerebellar cortico-nuclear motor connectivity that is between 1 and 1.5 times greater than that of non-motor connectivity. This motor dominance appears to be dramatically reduced in humans. We found that only ~23% of the surface was connected with lobules HIV, V, and VI. When converted into a multiplier, we therefore estimate that motor connectivity is reduced to ~0.60 times that of non-motor connectivity. Though we acknowledge that neither we nor the work of Strick and colleagues were able to track/label the entirety of the connections to the dentate nucleus, we provide here the first evidence for a shift in the ratio of connectivity of regions that have been shown to be anatomically connected to motor and non-motor cortex in non-human primates. Additional work with high resolution task-based functional imaging and diffusion tractography in the same individuals would be required to assess the degree of overlap between anatomically and functionally defined motor and non-motor regions of the cerebellum. Though a separate question, it may also be possible to combine functional and and diffusion imaging to reveal the finer details of body somatotopy on the superior surface of the dentate nucleus.

In the present study, we chose a classification and thresholding method that was conservative enough to allow regions of the dentate nucleus to remain unlabelled. This method was used to avoid classification that could potentially be driven by a limited set of streamlines and thus bias interpretation. As a result, our findings likely represent a lower-bound for areal classification of the human dentate nucleus. This effect is particularly visible on the supero-lateral surface, as seen in Figure 6, and is likely due to the presence of an orthogonal dominant fibre bundle in this region of the cerebellum, the MCP. The most direct path for fibres originating in the most postero-lateral aspects of the cerebellar cortex (primarily lobules HVI and Crus I) is through the MCP to terminate on the unlabelled superior portion of the lateral aspect of the dentate nucleus. Though it has previously been reported that dMRI-based fibre tractography is impossible in this region at lower spatial resolutions (Granziera et al. 2009), our results show that increased spatial resolution improves our ability to identify most, but not all, structural connectivity of the human dentate nucleus. Though we were able to successfully perform tractography between lobules HIV, V, VI and Crus I, II, the data quality in lobules VIIB and VIII was not sufficient to allow us to accurately characterise their cortico-nuclear connectivity. These lobules, thought to form a mirrored motor representation in the cerebellar cortex (Grodd et al. 2001) , are the furthest distance in the brain from the magnet isocenter. Even though dielectric pads were used to preserve signal homogeneity throughout the cerebellum, we were not able to recover comparable data quality in lobules VIIB and VIII. This effect can be seen in the TDI in the bottom panel of Figure 2 (red circle) and is also visible in the b0 images presented in Figure S1. However, since these regions are thought to account for only ~20% of the overall connectivity to the primary motor cortex in non-human primates (Kelly and Strick 2003), their removal is unlikely to significantly alter our results. Even with these caveats, our results also provide a much more complete and detailed picture of white-matter connectivity within the cerebellum that, with further improvement in diffusion-weighted acquisitions and tractography algorithms, should allow a complete mapping of connectivity between the cerebellum and cerebral cortex.

Methodological advances including higher b-values (Setsompop et al. 2013), oscillating gradients (Lundell et al. 2015), ex-vivo preparations with higher spatial resolution (Dell'Acqua et al. 2013), and tractography on histological cross-sections (Larsen et al. 2007; Budde and Annese 2013) are welcome complements to this work. High resolution ex-vivo datasets may be particularly useful for identifying the finer details of cortico-nuclear connectivity within individual lobules, including more fine-grained topographical mapping and the mapping of projection angles to the dentate nucleus. In particular, recent work has begun to tackle three-dimensional reconstructions of sub-100 micrometre polarised light imaging data to identify extremely fine white-matter anatomical details (Reckfort et al. 2015).The diffusion-weighted imaging data presented in this study is, to our knowledge, the highest in-vivo resolution acquired to date. Diffusion imaging at this spatial resolution provides the field with unique opportunities to resolve anatomical features and connectivity patterns that are indistinguishable at conventional resolutions. However, we must also recognise that there are limitations to

this technique. Even the highest ex-vivo spatial resolution is not able to provide the diffusion profile for an axon, or tens of axons, within a single voxel – but represents the average diffusion properties of the axons and cell bodies making up the underlying tissue microstructure (Jones 2008). Nevertheless, diffusion tractography is the only method for assessing three dimensional white-matter connectivity that can be repeatedly performed on live human subjects – and validation and interpretation is an active area of research (e.g., Dauguet et al. 2007; Thomas et al. 2014; Azadbakht et al. 2015). The present study used constrained spherical deconvolution and probabilistic tractography to better model and take into account the effects of crossing fibres. In addition, the high resolution and precise seed and target region identification enabled us to generate a probabilistic tractography path from the grey matter of the cortical lobules to the dentate nucleus. To be as specific as possible, we selected only those regions of the lobule that overlapped with the individual's cerebellar cortical mask and seeded tractography streamlines within the entire region. This method was able to exclude most white-matter bundles from the seeding mask to a much greater extent than would be possible at conventional resolutions. Thus, our results provide the most anatomically specific description of cerebellar organisation and the first description of cerebellar cortico-nuclear connectivity in the living human brain.

The strengths of diffusion imaging are in its ability to visualise connectivity in three dimensions, provide an overview of connectivity at a larger scale in a single individual (not possible with conventional tract-tracing), and to be performed on live subjects. High-resolution diffusion imaging of the human cerebellum has direct clinical applications (Perrini et al. 2012; Akakin et al. 2014) and contributes important insights to our understanding of intrinsic cerebellar and cortico-cerebellar organisation (Ramnani et al. 2006; Granziera et al. 2009; Dell'Acqua et al. 2013; Takahashi et al. 2013). Future work could take up the challenge of characterising the complete circuit of reciprocal connectivity between the cortex and cerebellum to provide further contributions to our understanding of the role of the cerebellum. Our findings are well aligned with previously described comparisons of SCP connectivity in humans and non-human primates (Ramnani et al. 2006). Since our study was only able to acquire diffusion images in the cerebellum and brainstem (Figure 1A) we are unable to comment on the topography of the connections to the cerebral cortex.

This study presents the first human evidence for a topographical pattern of white-matter connectivity between the cerebellar cortex and dentate nucleus – revealing an organisation that can help us to understand and probe the structure and functional significance of cortico-cerebellar loops in human behaviour. It presents the first evidence that a significant portion of the human dentate nucleus is dominated by non-motor connectivity, which is reversed in non-human primates, and further illustrates the importance of cortico-cerebellar loops in higher cognitive behaviour.

Acknowledgments

Author contributions

CJS designed the study with feedback from AA, NR, and AV. AS, R Trampel, AA, and CJS optimised the acquisition parameters and acquired the data. CJS, PLB, and AA created and/or adapted the software and scripts for analysis and CJS performed all data analysis with the input and assistance of AA and PLB. CJS prepared the manuscript with feedback from all co-authors.

References

Adamaszek M, D'Agata F, Kirkby KC, Trenner MU, Sehm B, Steele CJ, Berneiser J, Strecker K. 2014. Impairment of emotional facial expression and prosody discrimination due to ischemic cerebellar lesions. Cerebellum. 13:338–345.

Akakin A, Peris-Celda M, Kilic T, Seker A, Gutierrez-Martin A, Rhoton A. 2014. The dentate nucleus and its projection system in the human cerebellum: the dentate nucleus microsurgical anatomical study. Neurosurgery. 74:401–425.

Avants BB, Epstein CL, Grossman M, Gee JC. 2008. Symmetric diffeomorphic image registration with cross-correlation: evaluating automated labeling of elderly and neurodegenerative brain. Med Image Anal. 12:26–41.

Azadbakht H, Parkes LM, Haroon HA, Augath M, Logothetis NK, Crespigny A de, D'Arceuil HE, Parker GJM. 2015. Validation of high-resolution tractography against in vivo tracing in the macaque visual cortex. Cereb Cortex. 25:4299–4309.

Bazin P-L, Weiss M, Dinse J, Schäfer A, Trampel R, Turner R. 2014. A computational framework for ultra-high resolution cortical segmentation at 7 Tesla. Neuroimage. 93, Part 2:201–209.

Behrens TEJ, Johansen-Berg H, Woolrich MW, Smith SM, Wheeler-Kingshott C a. M, Boulby PA, Barker GJ, Sillery EL, Sheehan K, Ciccarelli O, Thompson AJ, Brady JM, Matthews PM. 2003. Non-invasive mapping of connections between human thalamus and cortex using diffusion imaging. Nat Neurosci. 6:750–757.

Bernard JA, Peltier SJ, Benson BL, Wiggins JL, Jaeggi SM, Buschkuehl M, Jonides J, Monk CS, Seidler RD. 2014. Dissociable functional networks of the human dentate nucleus. Cereb Cortex. 24:2151–2159.

Bodranghien F, Bastian A, Casali C, Hallett M, Louis ED, Manto M, Mariën P, Nowak DA, Schmahmann JD, Serrao M, Steiner KM, Strupp M, Tilikete C, Timmann D, van Dun K. 2016. Consensus paper: revisiting the symptoms and signs of cerebellar syndrome. Cerebellum. 15:369–391.

Buckner RL. 2013. The Cerebellum and Cognitive Function: 25 Years of Insight from Anatomy and Neuroimaging. Neuron. 80:807–815.

Buckner RL, Krienen FM, Castellanos A, Diaz JC, Yeo BTT. 2011. The organization of the human cerebellum estimated by intrinsic functional connectivity. J Neurophysiol. 106:2322–2345.

Budde MD, Annese J. 2013. Quantification of anisotropy and fiber orientation in human brain histological sections. Front Integr Neurosci. 7:3.

Calamante F, Tournier J-D, Heidemann RM, Anwander A, Jackson GD, Connelly A. 2011. Track density imaging (TDI): Validation of super resolution property. Neuroimage. 56:1259–1266.

Chan-Palay V. 1977. Cerebellar dentate nucleus. Springer Berlin Heidelberg.

Clarke RH, Horsley V. 1905. On the intrinsic fibres of the cerebellum, its nuclei and its efferent tracts. Brain. 28:13–29.

Dauguet J, Peled S, Berezovskii V, Delzescaux T, Warfield SK, Born R, Westin C-F. 2007. Comparison of fiber tracts derived from in-vivo DTI tractography with 3D histological neural tract tracer reconstruction on a macaque brain. Neuroimage. 37:530–538.

Dell'Acqua F, Bodi I, Slater D, Catani M, Modo M. 2013. MR diffusion histology and micro-tractography reveal mesoscale features of the human cerebellum. The Cerebellum. 12:923–931.

Deoni SCL, Catani M. 2007. Visualization of the deep cerebellar nuclei using quantitative T1 and ρ magnetic resonance imaging at 3 Tesla. Neuroimage. 37:1260–1266.

Diedrichsen J, Maderwald S, Küper M, Thürling M, Rabe K, Gizewski ER, Ladd ME, Timmann D. 2011. Imaging the deep cerebellar nuclei: A probabilistic atlas and normalization procedure. Neuroimage. 54:1786–1794.

Dimitrova A, Weber J, Redies C, Kindsvater K, Maschke M, Kolb FP, Forsting M, Diener HC, Timmann D. 2002. MRI atlas of the human cerebellar nuclei. Neuroimage. 17:240–255.

Dum RP, Li C, Strick PL. 2002. Motor and nonmotor domains in the monkey dentate. Ann N Y Acad Sci. 978:289–301.

Dum RP, Strick PL. 2003. An unfolded map of the cerebellar dentate nucleus and its projections to the cerebral cortex. J Neurophysiol. 89:634–639.

Glickstein M, Doron K. 2008. Cerebellum: Connections and Functions. Cerebellum. 7:589–594.

Granziera C, Schmahmann JD, Hadjikhani N, Meyer H, Meuli R, Wedeen V, Krueger G. 2009. Diffusion spectrum imaging shows the structural basis of functional cerebellar circuits in the human cerebellum in vivo. PLoS ONE. 4:e5101.

Grimaldi G, Argyropoulos GP, Boehringer A, Celnik P, Edwards MJ, Ferrucci R, Galea JM, Groiss SJ, Hiraoka K, Kassavetis P, Lesage E, Manto M, Miall RC, Priori A, Sadnicka A, Ugawa Y, Ziemann U. 2014. Non-invasive cerebellar stimulation--a consensus paper. Cerebellum. 13:121–138.

Grodd W, Hülsmann E, Lotze M, Wildgruber D, Erb M. 2001. Sensorimotor mapping of the human cerebellum: fMRI evidence of somatotopic organization. Hum Brain Mapp. 13:55–73.

Heidemann RM, Anwander A, Feiweier T, Knösche TR, Turner R. 2012. k-space and q-space: Combining ultra-high spatial and angular resolution in diffusion imaging using ZOOPPA at 7 T. Neuroimage. 60:967–978.

Jansen J, Brodal A. 1940. Experimental studies on the intrinsic fibers of the cerebellum. II. The cortico-nuclear projection. J Comp Neurol. 73:267–321.

Jones DK. 2008. Studying connections in the living human brain with diffusion MRI. Cortex. 44:936–952.

Kelly RM, Strick PL. 2003. Cerebellar loops with motor cortex and prefrontal cortex of a nonhuman primate. J Neurosci. 23:8432–8444.

Küper M, Dimitrova A, Thürling M, Maderwald S, Roths J, Elles HG, Gizewski ER, Ladd ME,Diedrichsen J, Timmann D. 2011. Evidence for a motor and a non-motor domain in the human dentate nucleus — An fMRI study. Neuroimage. 54:2612–2622.

Larsell O. 1970. The comparative anatomy and histology of the cerebellum from monotremes through apes. University of Minnesota Press.

Larsen L, Griffin LD, GRäßel D, Witte OW, Axer H. 2007. Polarized light imaging of white matter architecture. Microsc Res Tech. 70:851–863.

Lohmann G, Bohn S, Müller K, Trampel R, Turner R. 2010. Image restoration and spatial resolution in 7-Tesla magnetic resonance imaging. Magn Reson Med. 64:15–22.

Lucas BC, Kazhdan M, Taylor RH. 2012. Multi-Object Geodesic Active Contours (MOGAC). Med Image Comput Comput Assist Interv. MICCAI 2012. 15:404-412.

Lundell H, Sønderby CK, Dyrby TB. 2015. Diffusion weighted imaging with circularly polarized oscillating gradients. Magn Reson Med. 73:1171–1176.

Manjón JV, Coupé P, Concha L, Buades A, Collins DL, Robles M. 2013. Diffusion weighted image denoising using overcomplete local PCA. PLoS ONE. 8:e73021.

Marques JP, Kober T, Krueger G, van der Zwaag W, Van de Moortele P-F, Gruetter R. 2010. MP2RAGE, a self bias-field corrected sequence for improved segmentation and T1-mapping at high field. Neuroimage. 49:1271–1281.

Marvel CL, Desmond JE. 2010. Functional topography of the cerebellum in verbal working memory. Neuropsychol Rev. 20:271–279.

McAuliffe MJ, Lalonde FM, McGarry D, Gandler W, Csaky K, Trus BL. 2001. Medical image processing, analysis and visualization in clinical research. In: 14th IEEE Symposium on Computer-Based Medical Systems, 2001. CBMS 2001. p. 381–386.

Middleton FA, Strick PL. 2001. Cerebellar projections to the prefrontal cortex of the primate. J Neurosci. 21:700–712.

Mollink J, Baarsen KM van, Dederen PJWC, Foxley S, Miller KL, Jbabdi S, Slump CH, Grotenhuis JA, Kleinnijenhuis M, Walsum AM van C van. 2015. Dentatorubrothalamic tract localization with postmortem MR diffusion tractography compared to histological 3D reconstruction. Brain Struct Funct. 1–15.

O'Reilly JX, Beckmann CF, Tomassini V, Ramnani N, Johansen-Berg H. 2010. Distinct and overlapping functional zones in the cerebellum defined by resting state functional connectivity. Cereb Cortex. 20:953–965.

Perrini P, Tiezzi G, Castagna M, Vannozzi R. 2012. Three-dimensional microsurgical anatomy of cerebellar peduncles. Neurosurg Rev. 36:215–225.

Ramnani N. 2006. The primate cortico-cerebellar system: anatomy and function. Nat Rev Neurosci. 7:511–522.

Ramnani N, Behrens TEJ, Johansen-Berg H, Richter MC, Pinsk MA, Andersson JLR, Rudebeck P, Ciccarelli O, Richter W, Thompson AJ, Gross CG, Robson MD, Kastner S, Matthews PM. 2006. The evolution of prefrontal inputs to the cortico-pontine system: diffusion imaging evidence from macaque monkeys and humans. Cereb Cortex. 16:811–818.

Reckfort J, Wiese H, Pietrzyk U, Zilles K, Amunts K, Axer M. 2015. A multiscale approach for the reconstruction of the fiber architecture of the human brain based on 3D-PLI. Front Neuroanat. 9.

Rhoton AL. 2000. Cerebellum and fourth ventricle. Neurosurgery. 47:S7-27.

Schmahmann JD, MacMore J, Vangel M. 2009. Cerebellar stroke without motor deficit: Clinical evidence for motor and non-motor domains within the human cerebellum. Neuroscience. 162:852–861.

Sehm B, Taubert M, Conde V, Weise D, Classen J, Dukart J, Draganski B, Villringer A, Ragert P. 2014. Structural brain plasticity in Parkinson's disease induced by balance training. Neurobiol Aging. 35:232–239.

Setsompop K, Kimmlingen R, Eberlein E, Witzel T, Cohen-Adad J, McNab JA, Keil B, Tisdall MD,Hoecht P, Dietz P, Cauley SF, Tountcheva V, Matschl V, Lenz VH, Heberlein K, Potthast A, Thein H, Van Horn J, Toga A, Schmitt F, Lehne D, Rosen BR, Wedeen V, Wald LL. 2013. Pushing the limits of in vivo diffusion MRI for the Human Connectome Project. Neuroimage. 80:220–233.

Smith SM, Jenkinson M, Woolrich MW, Beckmann CF, Behrens TEJ, Johansen-Berg H, Bannister PR, De Luca M, Drobnjak I, Flitney DE, Niazy RK, Saunders J, Vickers J, Zhang Y, De Stefano N, Brady JM, Matthews PM. 2004. Advances in functional and structural MR image analysis and implementation as FSL. Neuroimage. 23:S208–S219.

Stoodley CJ, Schmahmann JD. 2009. Functional topography in the human cerebellum: A metaanalysis of neuroimaging studies. Neuroimage. 44:489–501.

Stoodley CJ, Schmahmann JD. 2010. Evidence for topographic organization in the cerebellum of motor control versus cognitive and affective processing. Cortex. 46:831–844.

Stoodley CJ, Valera EM, Schmahmann JD. 2012. Functional topography of the cerebellum for motor and cognitive tasks: an fMRI study. Neuroimage. 59:1560–1570.

Strick PL, Dum RP, Fiez JA. 2009. Cerebellum and nonmotor function. Ann Rev Neurosci. 32:413–434.

Sultan F, Hamodeh S, Baizer JS. 2010. The human dentate nucleus: a complex shape untangled. Neuroscience. 167:965–968.

Takahashi E, Song JW, Folkerth RD, Grant PE, Schmahmann JD. 2013. Detection of post-mortem human cerebellar cortex and white matter pathways using high angular resolution diffusion tractography: A feasibility study. Neuroimage. 68:105–111.

Teeuwisse WM, Brink WM, Webb AG. 2012. Quantitative assessment of the effects of highpermittivity pads in 7 Tesla MRI of the brain. Magn Reson Med. 67:1285–1293.

Thomas C, Ye FQ, Irfanoglu MO, Modi P, Saleem KS, Leopold DA, Pierpaoli C. 2014. Anatomical accuracy of brain connections derived from diffusion MRI tractography is inherently limited. Proc Natl Acad Sci U S A. 111:16574–16579.

Thürling M, Küper M, Stefanescu R, Maderwald S, Gizewski ER, Ladd ME, Timmann D. 2011. Activation of the dentate nucleus in a verb generation task: A 7T MRI study. Neuroimage. 57:1184–1191.

Tournier J-D, Calamante F, Connelly A. 2007. Robust determination of the fibre orientation distribution in diffusion MRI: Non-negativity constrained super-resolved spherical deconvolution. Neuroimage. 35:1459–1472.

van Baarsen KM, Kleinnijenhuis M, Jbabdi S, Sotiropoulos SN, Grotenhuis JA, van Cappellen van Walsum AM. 2016. A probabilistic atlas of the cerebellar white matter. Neuroimage. 124:724–732.

van Essen DC. 2013. Cartography and connectomes. Neuron. 80:775–790.

Voogd J, Shinoda Y, Ruigrok TJH, Sugihara I. 2013. Cerebellar Nuclei and the Inferior Olivary Nuclei: Organization and Connections. In: Handbook of the Cerebellum and Cerebellar Disorders. New York: Springer. p. 377–436.

Supplementary Materials

Table S1. Mean of the motion correction translation parameters for each participant.

	Translations (mm)		
	x	y	z
S1	0.23	0.16	0.31
S2	1.39	0.83	0.68
S3	0.42	0.38	1.17
S4	0.20	1.00	0.36
S5	0.93	0.23	2.60
S6	0.04	0.19	0.65

Table S2. Mean motion correction rotation parameters for each participant.

	Rotations (degrees)		
	x	y	z
S1	0.40	0.26	0.07
S2	0.38	0.00	1.14
S3	0.12	0.41	0.09
S4	1.43	0.32	0.75
S5	1.10	0.90	0.26
S6	1.06	0.12	0.02
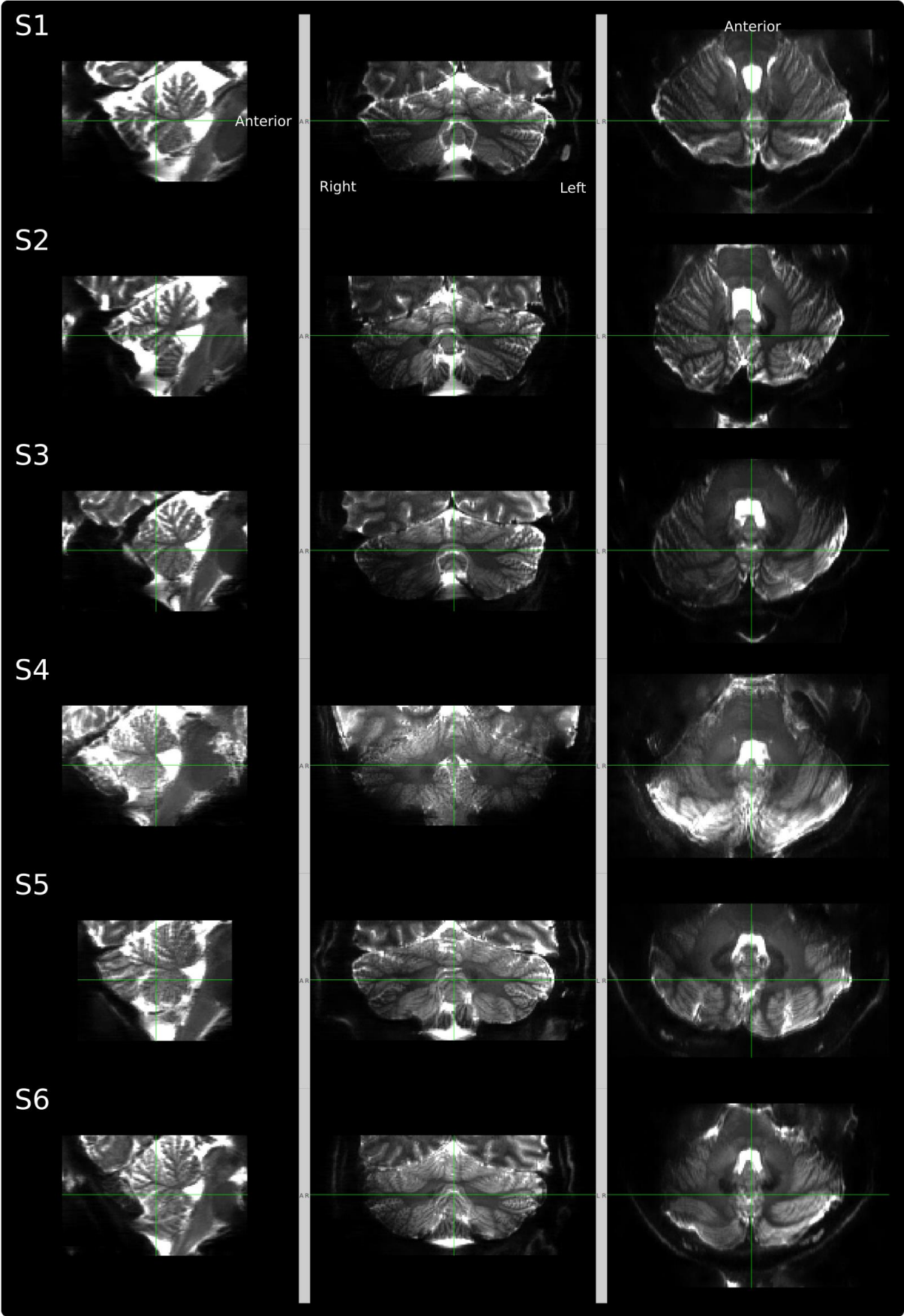
Figure S1. Mean of the denoised b0 images for each participant without motion correction. The participant with the largest

amount of rotation produced images with the most blurring in the cerebellar cortex and decreased contrast over the entire field of view (S4). We could detect no differences in the tractography and classification results in this or any participant when compared with the rest of the group.
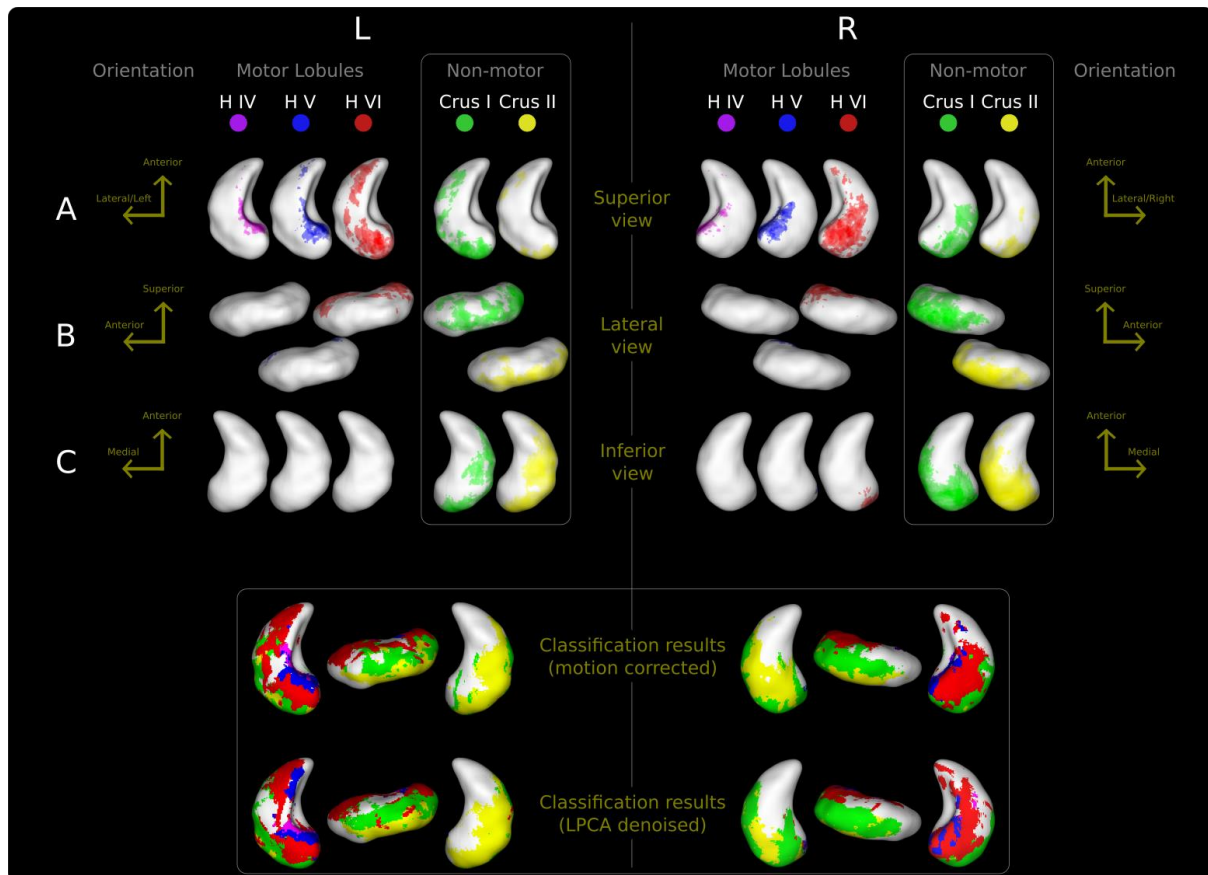
Figure S2. Motion corrected replication of the results shown in Figure 5 of the manuscript (without 4d LPCA denoising). The distribution of connectivity for each of the lobules, and the overlap and distinctions within and between the motor and non-motor lobules, is virtually identical to the results obtained without motion correction (with 4d LPCA denoising). The classification results with motion correction (no 4d LPCA denoising) shown in the bottom panel are also virtually the same as those with 4d LPCA denoising (no motion correction). This panel includes images of the 4d LPCA denoised classification included in Figures 5 and 6 of the manuscript for direct comparison.